THE FIRST MILLIMETER DETECTION OF A NON-ACCRETING ULTRACOOL DWARF

P. K. G. WILLIAMS[1], S. L. CASEWELL[2], C. R. STARK[3], S. P. LITTLEFAIR[4], CH. HELLING[5], AND E. BERGER[1]

[1] Harvard-Smithsonian Center for Astrophysics, 60 Garden Street, Cambridge, MA 02138, USA; pwilliams@cfa.harvard.edu
[2] Department of Physics and Astronomy, University of Leicester, University Road, Leicester LE1 7RH, UK
[3] Division of Computing and Mathematics, Abertay University, Dundee DD1 1HG, UK
[4] Department of Physics and Astronomy, University of Sheffield, Sheffield S3 7RH, UK
[5] SUPA, School of Physics and Astronomy, University of St Andrews, St Andrews KY16 9SS, UK

ABSTRACT

The well-studied M9 dwarf TVLM 513–46546 is a rapid rotator ($P_{\rm rot} \sim 2$ hr) hosting a stable, dipolar magnetic field of ~ 3 kG surface strength. Here we report its detection with ALMA at 95 GHz at a mean flux density of $56 \pm 12\,\mu$Jy, making it the first ultracool dwarf detected in the millimeter band, excluding young, disk-bearing objects. We also report flux density measurements from unpublished archival VLA data and new optical monitoring data from the Liverpool Telescope. The ALMA data are consistent with a power-law radio spectrum that extends continuously between centimeter and millimeter wavelengths. We argue that the emission is due to the synchrotron process, excluding thermal, free–free, and electron cyclotron maser emission as possible sources. During the interval of the ALMA observation that phases with the maximum of the object's optical variability, the flux density is higher at a $\sim 1.8\sigma$ significance level. These early results show how ALMA opens a new window for studying the magnetic activity of ultracool dwarfs, particularly shedding light on the particle acceleration mechanism operating in their immediate surroundings.

Key words: brown dwarfs – radio continuum: stars – stars: individual (TVLM 513–46546)

1. INTRODUCTION

It has long been recognized that both stars and giant planets possess magnetic fields (Hale 1908; Zhelezniakov 1958). The Sun and the planets have very different magnetic phenomenologies, however, making it unclear what kind of magnetic activity—if any (Mohanty et al. 2002)—should be expected for objects with masses between these extremes. Only relatively recently have observations made it clear that intermediate-mass objects can host vigorous magnetic activity that has characteristics reminiscent of *both* of these regimes (Berger et al. 2001, 2010; Berger 2006; Hallinan et al. 2006, 2015; McLean et al. 2012; Williams et al. 2014). The study of magnetic activity in ultracool dwarfs (stars and brown dwarfs with spectral types ≥M7; Kirkpatrick et al. 1999; Martín et al. 1999) not only provides insight into the internal structures and local environments of these objects (e.g., Nichols et al. 2012; Stassun et al. 2012), but also leads the way toward analogous studies of exoplanets themselves, which have thus far eluded detection despite significant efforts (e.g., Lazio & Farrell 2007; Lecavelier des Etangs et al. 2011).

Radio observations have been the chief observational tool for understanding magnetism in the ultracool regime. This is in part because other standard tracers (e.g., X-ray and Hα emission) become difficult to measure in these faint, rapidly rotating objects (Gizis et al. 2000; Stelzer et al. 2006; Berger et al. 2010; Williams et al. 2014; Schmidt et al. 2015), but also because radio observations reveal an enticing and puzzling phenomenology. Bright, highly polarized, periodic pulses are interpreted as auroral phenomena, specifically bursts due to the electron cyclotron maser instability (ECMI; Wu & Lee 1979; Treumann 2006) that diagnose large-scale magneto/ionospheric current systems (Hallinan et al. 2006; Lynch et al. 2015). For reasons that are poorly understood, however, pulse structures vary on both short and long timescales, sometimes disappearing

completely (Berger et al. 2008; Williams & Berger 2015). Meanwhile, the broadband non-flaring ("quasi-quiescent") emission from these objects is reminiscent of gyrosynchrotron emission from active stars, but often has an unusually flat spectrum ($0 < \alpha < -0.5$, $S_\nu \propto \nu^\alpha$), can have significant polarization, and seemingly occurs at a spectral luminosity that is independent of bolometric luminosity (Hallinan et al. 2008; Osten et al. 2009; McLean et al. 2011). In some sources this emission appears steady over $\sim$year timescales (Osten et al. 2009) while in others it varies significantly (factor-of-two changes; Antonova et al. 2007, 2010); to date radio monitoring has not been consistent enough to shed light on the relevant evolutionary timescales, which could potentially reflect magnetic activity cycles (Saar & Brandenburg 1999). Another major puzzle is the origin of the energetic electrons driving the ECMI bursts; two proposed sources are atmospheric ionization processes (Helling et al. 2011) and magneto-ionospheric coupling currents (Nichols et al. 2012).

Modern radio telescopes are capable of achieving $\sim\mu$Jy sensitivities at high frequencies ($\gtrsim 20$ GHz), raising the possibility of probing the means by which particles are accelerated to MeV energies by objects with effective temperatures of $\lesssim 2500$ K. Here we present a detection of the ultracool dwarf TVLM 51346546 (hereafter TVLM 513) at 95 GHz with the Atacama Large Millimeter/submillimeter Array (ALMA), the first such result at millimeter wavelengths.[6]

We proceed by summarizing the characteristics of TVLM 513 (Section 2), then describing our observations and data reduction (Section 3). We next discuss some intriguing features in the data (Section 4). Finally we present our conclusions (Section 5).

---

[6] Here and throughout this work we disregard millimeter detections of disks around young ultracool dwarfs (e.g., Kraus et al. 2015).

2. THE ULTRACOOL DWARF TVLM 513–46546

TVLM 513 was first determined to be a nearby, faint star by Tinney (1993) through trigonometric parallax measurements. Kirkpatrick et al. (1995) originally adopted a spectral type of M8.5, but both Reid et al. (2008) and West et al. (2011) update the assignment to M9. Astrometric VLBI monitoring has yielded a precise trigonometric parallax implying a distance of 10.762 ± 0.027 pc (Forbrich et al. 2013) and an absolute K_s-band (2MASS; Skrutskie et al. 2006) magnitude of 10.547 ± 0.025 mag. A lack of Li absorption lines implies an age $\gtrsim 100$ Myr, and in connection, a mass $\gtrsim 0.06 \, M_\odot$ (Martín et al. 1994; Reid et al. 2002), while membership in the "young/old disk" kinematic category of Leggett (1992) is suggested by a low space velocity (Leggett et al. 1998). The VLBI astrometry excludes the presence of unseen companions with masses $\gtrsim 4 \, M_J$ at orbital periods $\gtrsim 10$ day or with masses $\gtrsim 0.3 \, M_J$ at periods $\gtrsim 710$ day (Forbrich et al. 2013). NIR imaging excludes companions with separations between 0.1 and 15 arcsec (Close et al. 2003).

While it has relatively weak Hα emission (EW$_{H\alpha} \sim 2$ Å; Martín et al. 1994; Basri 2001), TVLM 513 is one of the most-observed radio-active ultracool dwarfs (Berger 2002; Hallinan et al. 2006, 2007; Osten et al. 2006; Berger et al. 2008; Forbrich & Berger 2009; Doyle et al. 2010; Jaeger et al. 2011; Forbrich et al. 2013; Wolszczan & Route 2014; Lynch et al. 2015). Its non-flaring flux density varies at the 30% level over ~year timescales (Antonova et al. 2010). Both Osten et al. (2006) and Hallinan et al. (2007) report quasi-simultaneous flux density measurements of TVLM 513 at multiple frequencies, providing insight as to the shape of its broadband spectrum, as explored below.

Additionally, TVLM 513 usually emits periodic ECMI flares that allow measurement of its rotation period, P_{rot}, and surface field strength (Hallinan et al. 2006). Doyle et al. (2010) used these flares to measure $P_{rot} = 1.96733 \pm 0.00002$ hr, consistent with spectroscopic measurements of $v \sin i \sim 60$ km s^{-1} (Basri 2001; Mohanty & Basri 2003). TVLM 513 is also optically variable at the ~10 mmag level in the I band at the same periodicity (Lane et al. 2007). This variability is recovered in the SDSS i' and g' bands with an 180° phase shift between the two (Littlefair et al. 2008), which was originally interpreted as signifying the presence of a dust cloud but may be associated with TVLM 513's known auroral phenomena (Hallinan et al. 2015). Five years of I and i' band monitoring by Harding et al. (2013) lead them to measure $P_{rot} = 1.95958 \pm 0.00005$ hr with stable phasing over that time period. They find a peak-to-peak variability amplitude that varies with time between ~0.6 and 1.2%. Wolszczan & Route (2014) combine the radio and optical data to obtain a consistent value, $P_{rot} = 1.959574 \pm 0.000002$ hr. Most recently, Miles-Páez et al. (2015) report periodic variation in the linear polarization of TVLM 513's optical emission at a ~65° phase difference from the total intensity, suggesting the presence of free electrons close to the object ($d \lesssim R_*$) or inhomogeneous dust structures, as suggested by Littlefair et al. (2008).

3. OBSERVATIONS AND DATA REDUCTION

3.1. ALMA

TVLM 513 was observed with ALMA on UT date 2015 April 03 (proposal 2013.1.00293.S, PI: Casewell) using the "band 3" receivers (~100 GHz observing frequency) in the
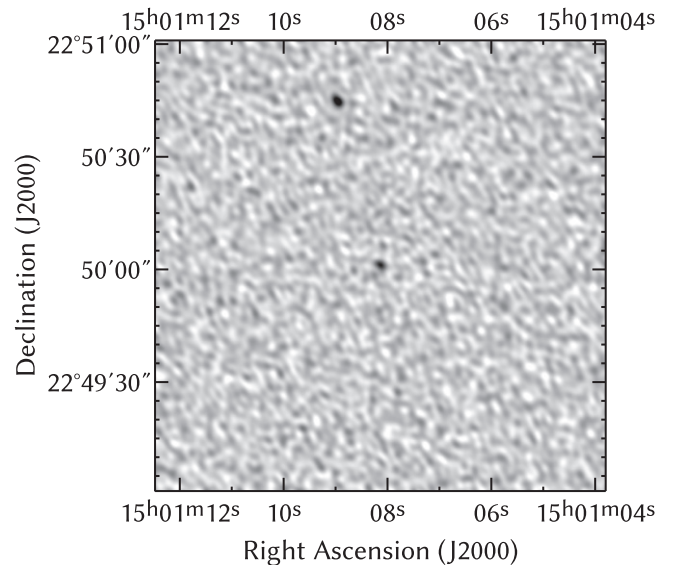
Figure 1. ALMA detection image of TVLM 513. The effective frequency of the image is 97.48 GHz, the total bandwidth is 8 GHz, the grayscale runs from $-20 \, \mu$Jy (white) to 65 μJy (black), and the image rms is ~8.4 μJy. A source is detected at the expected position of TVLM 513 with a flux density of $55 \pm 12 \, \mu$Jy, where the uncertainty in the flux density comes from least-squares fitting the pixel data. The synthesized beam is 3.1×2.2 arcsec at a position angle of 44°.

standard wideband continuum mode. The correlator recorded data for two sidebands centered on 91.46 GHz (lower sideband, LSB) and 103.49 GHz (upper sideband, USB), each having a total bandwidth of 4 GHz. The observations lasted just under 4 hr, with the total on-source integration time being 2.15 hr. Full Stokes correlations were not obtained, precluding a polarimetric analysis.

Calibrated visibilities and a preliminary image were provided to us by the European ALMA Regional Center (EARC) after reduction by their staff. We examined the data and identified no lingering problems. Figure 1 shows the result of our re-imaging of the full data set, using a somewhat larger field of view than the EARC analysis.

Using the astrometric parameters reported by Forbrich et al. (2013), the expected position of TVLM 513 at the time of the ALMA observations was R.A. = 15:01:08.1463, decl. = +22:50:01.224, with an approximate uncertainty of 1 mas. In the ALMA image we find a source that is 6.2σ above the background noise at a position of R.A. = 15:01:08.139, decl. = +22:50:01.14. Fitting a source model to the image, we measure a flux density of $56 \pm 12 \, \mu$Jy and a positional uncertainty of 0.5 arcsec, where the uncertainty on the flux density is higher than the image rms (9 μJy) because it includes covariances with the source positions. The positions are consistent to 0.2σ, and we identify this source with TVLM 513.

We imaged the two ALMA sidebands separately to assess the spectral index of TVLM 513 at millimeter wavelengths. Our results are summarized in Table 1. In the LSB image, with an effective frequency of 91.46 GHz, the flux density of the source is $66 \pm 8 \, \mu$Jy. In the USB image, with an effective frequency of 103.49 GHz, it is $31 \pm 18 \, \mu$Jy. The rms of the latter image is ~12 μJy, so that the signal is at the 2.6σ level. The spectral index inferred from the ALMA data alone is $\alpha_{mm} \approx -5 \pm 4$, largely unconstrained but inconsistent at the

Table 1
New Flux Density Measurements of TVLM 513

Frequency (GHz)	Flux Density (μJy)	Obs. Date (BMJD)	Facility
(1)	(2)	(3)	(4)
1.57	217 ± 153	55546.51	VLA
6.10	214 ± 18	55546.50	VLA
19.75	136 ± 43	55546.49	VLA
91.46	66 ± 8	57115.24	ALMA
103.49	31 ± 18	57115.24	ALMA

97% confidence level with thermal emission, defined here as $\alpha \geqslant 1.5$ (Andrews & Williams 2005).

We extracted light curves from the calibrated LSB, USB, and band-averaged ALMA visibilities using the technique described in Williams et al. (2013), subtracting the lone additional source visible in the image from the visibilities. The resulting raw light curves have a sampling cadence of 2 s. The top panel of Figure 2 shows the LSB light curve after averaging to a bin size of 102 s, splitting bins across individual scans. We are unable to find conclusive evidence for variability, although there is a possible flux density increase around BMJD 57115.265 that we discuss below.

3.2. Archival VLA Data

We also analyzed unpublished archival observations of TVLM 513 performed with the Karl G. Jansky Very Large Array (VLA). TVLM 513 was observed at three frequencies on UT date 2010 December 16 while the VLA upgrade was being performed (project ID TRSR0033, PI: Hallinan). Three sequential observations were performed in K band ($\sim$20 GHz), C band ($\sim$6 GHz), and L band ($\sim$1.5 GHz) over the course of 1 hr. In the K band observation, data were taken in two basebands with center frequencies of 19.0 and 20.5 GHz and bandwidths of 1.024 GHz each. The C band observation used the same configuration with center frequencies of 4.8 and 7.4 GHz. The L band observation had two basebands of 0.512 MHz bandwidth configured contiguously, resulting in an effective spectral window of width 1.024 GHz centered at 1.58 GHz. In all cases individual spectral channels were 2 kHz wide. 3C 286 was the bandpass and flux density calibrator and 4C 23.41 was the complex gain calibrator.

We calibrated the data using standard procedures in the CASA software system (McMullin et al. 2007). We used the aoflagger tool to automatically flag radio-frequency interference (Offringa et al. 2010, 2012) and set the flux density scale using the preliminary, 2010 version of the scale defined by Perley & Butler (2013). From fitting a point-source model to images generated from data in the three bands, we obtain the flux densities reported in Table 1. The flux density measurement in L band is marginal but consistent with prior observations (Osten et al. 2006).

3.3. Liverpool Telescope

We observed TVLM 513 using IO:O on the fully robotic 2-m Liverpool Telescope (LT) on La Palma, on the night of 2015 August 5th (UT). We used the Sloan Digital Sky Survey (SDSS) i' filter with exposure times of 60 s. We bias-subtracted the images using the CCD overscan region and used twilight sky flats for flat field correction.
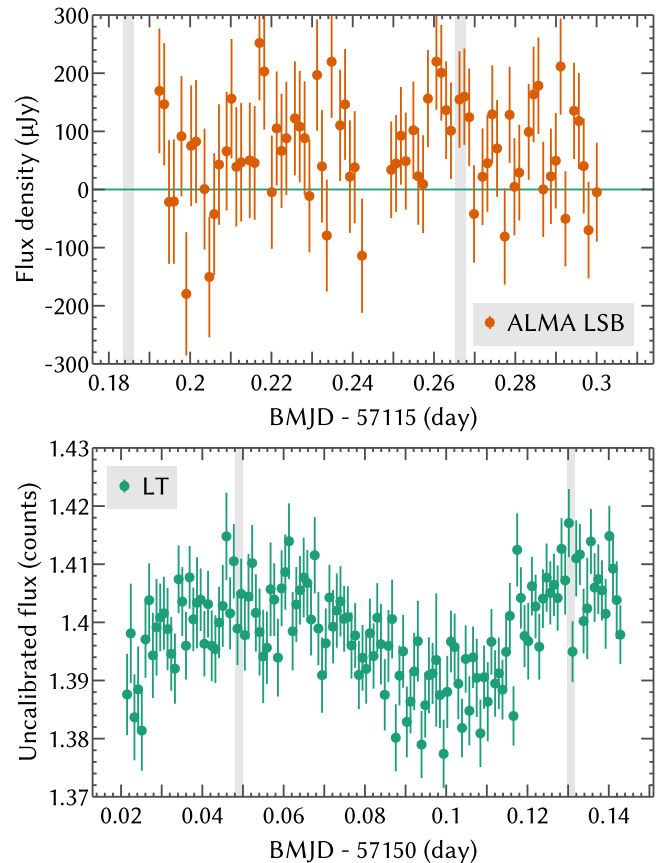
Figure 2. Light curves of TVLM 513 in millimeter (ALMA LSB; upper panel) and optical (lower panel) bands. The sampling intervals are 102 and 78 s, respectively. Both panels have widths of 3.31 hr. The vertical gray bands indicate the 1σ confidence bounds on the time of optical maximum as derived empirically from the LT data and propagated assuming a period of 1.95958 ± 0.00005 hr (Harding et al. 2013). The ALMA observations occurred 426 rotations prior to the LT observations. The possible increase in millimeter emission at BMJD 57115.265 occurs at the time of optical maximum.

We extracted fluxes for TVLM 513 and four nearby comparison stars using apertures whose sizes were scaled to 1.6 times the measured seeing in each image. Average seeing was $2''$, and the seeing ranged between $1''.6$ and $4''$. Conditions were photometric and all data were taken below an airmass of 1.15. We used the brightest two comparison stars to correct the data for transparency variations. We plot the LT optical light curve in the lower panel of Figure 2.

We measured the time of optical maximum in the LT light curve to be BMJD = 57150.049 ± 0.001 by fitting a sinusoid to the data, constraining the period to match the value determined by Wolszczan & Route (2014). The combined radio/optical ephemeris described in that work predicts an optical maximum at BMJD = 57150.028 (A. Wolszczan 2015, private communication), $\sim$90° out of phase with our observations.

4. DISCUSSION

Millimeter detections of stars are almost universally obtained from hot stars with winds and/or shells, young stars with disks, or giants with extremely large ($\sim$AU) photospheres at millimeter wavelengths (Altenhoff et al. 1994; Pallavicini & White 1996). While coronal-type emission has been suggested

as a target for mm observations, we are able to locate only a few robust detections at $\nu \gtrsim 90$ GHz in the literature; these are of either active binaries and/or flares (Bower et al. 2003; Brown & Brown 2006; Salter et al. 2008). We can locate no such published detections of single dMe flare stars, although to the best of our knowledge the lack of ALMA detections of these sources is due to a lack of observations rather than insufficient sensitivity.

4.1. Emission Mechanism

The $\gtrsim 100$ Myr age implied by the lack of Li absorption in TVLM 513 (Martín et al. 1994; Reid et al. 2002) is significantly longer than typical disk dissipation timescales of ~ 10 Myr (although there is evidence that disk lifetimes are inversely correlated with [sub]stellar mass; e.g., Williams & Cieza 2011). Furthermore, TVLM 513 does not have reported IR excesses, and the spectral index of the ALMA data is not consistent with the $\alpha \approx 2$ expected from thermal (photospheric or disk) emission (Reid & Menten 1997; Andrews & Williams 2005). We therefore reject this origin for the ALMA emission.

Topka & Marsh (1982) consider the relationship between X-ray emission and free–free radio emission from the active M4+M5 binary EQ Peg. Assuming parameters appropriate for active low-mass stars, they find that $S_{\nu,\mathrm{ff}} = (10^6 \,\mathrm{Jy}) f_X$, where f_X is measured over the 0.2–4 keV band in units of erg s^{-1} cm^{-2}. Applying TVLM 513's measured X-ray flux of $\sim 6 \times 10^{-16}$ erg s^{-1} cm^{-2} (Berger et al. 2008) and ignoring minor factors such as the chosen X-ray band, we estimate a negligible free–free contribution of $S_{\nu,\mathrm{ff}} \approx 1$ nJy. While this value is calculated for centimeter wavelength emission, the flat spectrum associated with optically thin free–free emission implies that it holds at mm wavelengths as well.

ECMI emission occurs predominantly at the cyclotron frequency $\nu_c = eB/2\pi m_e c$, requiring the presence of a magnetic field of $\gtrsim 34$ kG strength to explain the millimeter detections. This would be an order of magnitude stronger than any directly measured magnetic fields in low-mass stars (Reiners & Basri 2007, 2010; Morin et al. 2010) and exceeds theoretical limits on the surface field strengths associated with fully convective dynamos of ~ 3 kG (from energy equipartition with convective motions; Feiden & Chaboyer 2014). Therefore we reject an ECMI origin for this emission.

Having eliminated these other options, we conclude that the observed ALMA emission is synchrotron emission associated with TVLM 513's magnetic activity, as detailed below. Our results represent one of a handful of detections of such emission from single dwarfs at ALMA frequencies (84–950 GHz), ultracool or not (Bower et al. 2003). If additional observations constrain the brightness temperature of the millimeter emission to be implausibly large for the gyrosynchrotron process (e.g., detection of a rapid, bright burst), the previous paragraph implies that non-ECMI coherent processes such as the antenna mechanism (e.g., Komesaroff 1970) or plasma emission (e.g., Ginzburg & Zheleznia-kov 1958) should be considered.

4.2. The Broadband Radio Spectrum of TVLM 513

In Figure 3 we assemble a composite centimeter-to-millimeter spectrum of TVLM 513 from available simultaneous and quasi-simultaneous data. All published radio observations
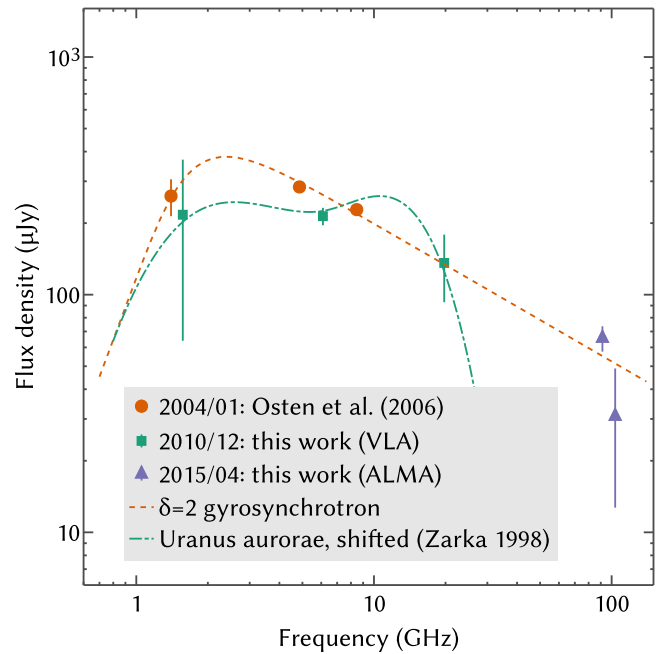
Figure 3. Non-simultaneous centimeter-to-millimeter spectrum of TVLM 513. The orange points show the data obtained quasi-simultaneously by Osten et al. (2006); green points show the quasi-simultaneous VLA data described in Section 3.2; blue points show the simultaneous ALMA data described in Section 3.1. The dashed lines show two representative spectral models described in Section 4.2; they disregard the long time baseline between the relevant VLA and ALMA observations and should not be used for quantitative analysis.

of TVLM 513 lie within this frequency range, with the exception of a 2.5σ upper limit of $S_\nu < 795$ μJy at 325 MHz (Jaeger et al. 2011). TVLM 513 is variable at the $\sim 30\%$ level over long ($\gtrsim$month) timescales (Antonova et al. 2010), so that inferences about the radio spectrum made by combining non-contemporaneous observations should be treated cautiously. The results of Osten et al. (2006) and the VLA analysis we present both suggest a spectrum peaking between 2 and 4 GHz with $\alpha \approx -0.4$ at higher frequencies. In contrast, Hallinan et al. (2007) report quasi-simultaneous observations at 4.88 and 8.44 GHz indicating a rising spectrum. However, their observations were made one day apart, so that variability may play a role in this finding. Furthermore, the flux densities they report average over several bright, polarized flares that are significantly brighter at the higher frequency. Using their Figure 3 to estimate the bias caused by these flares, we infer that the non-flaring spectrum in their observations has $\alpha \approx -0.1$.

In Figure 3 we show two possible models for the broadband spectrum of TVLM 513. We emphasize that these examples connect observations made years apart and so should not be used for quantitative analysis. In orange, we show a standard gyrosynchrotron model based on the equations of Dulk (1985), fit to our ALMA data and the measurements of Osten et al. (2006). Here we fixed $B = 100$ G and the electron energy spectral index $\delta = 2$, where $dN/dE \propto E^{-\delta}$, which leads to $\alpha = -0.5$ in the optically thin limit. Our ALMA data are consistent with a model in which the optically thin portion of spectrum extends all the way to the ALMA band. In this picture there is a hint of a spectral cutoff in the ALMA band. From the ALMA measurements, however, we calculate a $\sim 12\%$ chance that $\alpha_{\mathrm{mm}} > -0.5$, i.e., that the millimeter spectrum is at least as

flat as that observed at centimeter wavelengths. Fixing the known distance of TVLM 513 and the properties of our LSB detection, we infer a brightness temperature $T_B \sim (10^{6.4}\,\mathrm{K})(r/R_J)^{-2}$, where r is the characteristic length of the emitting region (Dulk 1985). This is consistent with gyrosynchrotron emission in the optically thin regime unless $r \lesssim 0.003\,R_J$.

Hallinan et al. (2006, 2008) have suggested that the broadband, non-flaring radio emission of ultracool dwarfs may be due to the ECMI rather than the gyrosynchrotron process, if there is continuous particle acceleration across a range of magnetic field strengths and propagation effects depolarize the emission. Osten et al. (2009) have used the plasma properties inferred from multi-band observations to argue against this interpretation for the binary LP 349–25 AB, and Ravi et al. (2011) analyze the broadband (5–24 GHz) radio spectrum of DENIS-P J104814.9–395604 to argue similarly. As argued above, our detection challenges this interpretation for TVLM 513 as well. To represent the sort of spectrum that might result from such an emission mechanism, in Figure 3 we show a version of the spectrum of Uranus' kilometric radiation (UKR) as shown by Zarka (1998), where both the emission frequencies and luminosities have been scaled arbitrarily to overlap the VLA measurements reported in Table 1. While this is just one possible example, it is representative of solar system observations (Zarka 1998). Although the preexisting data could have been consistent with such a spectral shape, the ALMA data exclude it.

4.3. Phased Millimeter and Optical Variability?

We do not find statistically significant evidence for variability in the millimeter emission. While the data show a ~15-minute period of elevated emission around BMJD = 57115.265, we cannot exclude the possibility that this elevated period is a noise fluctuation, given the duration of the observation and measurement scatter. A simple likelihood ratio test comparing a constant model and one with an exponentially fading flare yields an empirical p-value of ~7% (~1.8σ); i.e., in about 7% of simulated realizations of the constant model, the likelihood ratio of the best-fit flaring and constant models is least as high as that observed. Therefore the constant model cannot be rejected with confidence. An alternative Bayes factor analysis yields compatible results. The best-fit flare model achieves a peak flux density ~220 μJy above the quiescent level.

Confidence in this possible signal could be increased if it were periodic and observed multiple times, but the ALMA observation spanned only ~1.3 rotations of TVLM 513 and the timing of the putative event prevents this check. If the flare is real, it phases up with the maxima of TVLM 513's optical variability as revealed by our LT observations (Figure 2). Additional ALMA observations covering multiple rotation periods, paired with contemporaneous optical monitoring, could easily resolve whether the millimeter emission is periodically variable and how it might phase relative to the optical emission. If the possible variation is real and periodic, it would be out of phase with the polarized cm bursts, which differ in phase from the optical maxima by 0.41 ± 0.02 of a period (Wolszczan & Route 2014).

5. CONCLUSIONS

Our detection of TVLM 513 with ALMA makes it the first non-accreting ultracool dwarf to be detected at millimeter wavelengths. This detection bolsters the case for a gyrosynchrotron origin for the non-flaring radio emission of ultracool dwarfs, although in this case, as in previous work without such a large lever arm on the spectral index (Osten et al. 2006), a relatively shallow electron energy index $\delta = 2$ is inferred. At the high frequencies probed by ALMA, synchrotron cooling times are likely comparable to observational durations: an ambient field strength $B \gtrsim 40\,\mathrm{G}$ would lead to a cooling time shorter than the span of time on-source in this observation (2.6 hr; Petrosian 1985). For comparison, analyses of radio spectra have concluded $B \approx 100\,\mathrm{G}$ in NLTT 33370 AB (McLean et al. 2011) and $70 < B/\mathrm{G} < 260$ in DENIS-P J104814.9–395604 (Ravi et al. 2011). Osten et al. (2006) determined $B \lesssim 500\,\mathrm{G}$ in TVLM 513. Approximating synchrotron-emitting electrons to emit at the frequency $\gamma^2 \nu_c$, the observed ALMA emission originates in electrons with $\gamma \sim 180(B/\mathrm{G})^{-1/2}$. Monitoring observations can therefore likely probe the fine-grained time dependence of the mechanism that injects energetic particles into TVLM's surroundings, about which little is currently known.

However, confident inferences based on the broadband radio spectrum of TVLM 513 are precluded because the ALMA observations were not obtained contemporaneously with observations at longer wavelengths, and TVLM 513's radio luminosity, and possibly its radio spectral shape, are variable. Additional support from the Joint ALMA Observatory to allow simultaneous observations with other observatories would be highly valuable. We note that the observations in this work were performed in ALMA's "Band 3," which is less subject to weather restrictions than its higher frequencies. Similarly, there are hints that there may be a periodic component in the millimeter emission of TVLM 513. In this particular case, the precisely measured rotation period makes it relatively easy to phase-connect observations obtained in widely spaced epochs, but given the possibly rapid evolution of emission in the ALMA band and a desire to investigate objects that are not as well-characterized, support from the Observatory for longer continuous observations would likewise be of great importance to future studies.

Finally, we note that these results could only be obtained thanks to ALMA's superior sensitivity compared to any previous millimeter-band instrument. This first detection marks the opening of a new window for intensive investigations of the magnetic dynamo and particle acceleration processes that are jointly responsible for the centimeter-to-millimeter emission of ultracool dwarfs.

REFERENCES

Altenhoff, W. J., Thum, C., & Wendker, H. J. 1994, A&A, 281, 161
Andrews, S. M., & Williams, J. P. 2005, ApJ, 631, 1134
Antonova, A., Doyle, J. G., Hallinan, G., Golden, A., & Bourke, S. 2010, BlgAJ, 14, 58
Antonova, A., Doyle, J. G., Hallinan, G., Golden, A., & Koen, C. 2007, A&A, 472, 257
Astropy Collaboration, Robitaille, T. P., Tollerud, E. J., et al. 2013, A&A, 558, 33
Basri, G. 2001, in ASP Conf. Ser. 223, 11th Cambridge Workshop on Cool Stars, Stellar Systems and the Sun, ed. R. J. García López, R. Rebolo & M. R. Zapatero Osorio (San Francisco, CA: ASP), 261
Berger, E. 2002, ApJ, 572, 503
Berger, E. 2006, ApJ, 648, 629
Berger, E., Ball, S., Becker, K. M., et al. 2001, Natur, 410, 338
Berger, E., Basri, G., Fleming, T. A., et al. 2010, ApJ, 709, 332
Berger, E., Gizis, J. E., Giampapa, M. S., et al. 2008, ApJ, 673, 1080
Bower, G. C., Plambeck, R. L., Bolatto, A., et al. 2003, ApJ, 598, 1140
Brown, J. M., & Brown, A. 2006, ApJ, 638, L37
Close, L. M., Siegler, N., Freed, M., & Biller, B. 2003, ApJ, 587, 407
Doyle, J. G., Antonova, A., Marsh, M. S., et al. 2010, A&A, 524, 15
Dulk, G. A. 1985, ARA&A, 23, 169
Feiden, G. A., & Chaboyer, B. 2014, ApJ, 789, 53
Forbrich, J., & Berger, E. 2009, ApJL, 706, L205
Forbrich, J., Berger, E., & Reid, M. J. 2013, ApJ, 777, 70
Ginzburg, V. L., & Zhelezniakov, V. V. 1958, SvA, 2, 653
Gizis, J. E., Monet, D. G., Reid, I. N., et al. 2000, AJ, 120, 1085
Hale, G. E. 1908, ApJ, 28, 315
Hallinan, G., Antonova, A., Doyle, J. G., et al. 2006, ApJ, 653, 690
Hallinan, G., Antonova, A., Doyle, J. G., et al. 2008, ApJ, 684, 644
Hallinan, G., Bourke, S., Lane, C., et al. 2007, ApJL, 663, L25
Hallinan, G., Littlefair, S., Cotter, G., et al. 2015, Natur, 523, 568
Harding, L. K., Hallinan, G., Boyle, R. P., et al. 2013, ApJ, 779, 101
Helling, C., Jardine, M., Witte, S., & Diver, D. A. 2011, ApJ, 727, 4
Jaeger, T. R., Osten, R. A., Lazio, T. J., Kassim, N., & Mutel, R. L. 2011, AJ, 142, 189
Kirkpatrick, J. D., Henry, T. J., & Simons, D. A. 1995, AJ, 109, 797
Kirkpatrick, J. D., Reid, I. N., Liebert, J., et al. 1999, ApJ, 519, 802
Komesaroff, M. M. 1970, Natur, 225, 612
Kraus, A. L., Andrews, S. M., Bowler, B. P., et al. 2015, ApJL, 798, L23
Lane, C., Hallinan, G., Zavala, R. T., et al. 2007, ApJL, 668, L163
Lazio, T. J. W., & Farrell, W. M. 2007, ApJ, 668, 1182
Lecavelier, A., Sirothia, S. K., Gopal-Krishna, & Zarka, P. 2011, A&A, 533, 50
Leggett, S. K. 1992, ApJS, 82, 351
Leggett, S. K., Allard, F., & Hauschildt, P. H. 1998, ApJ, 509, 836
Littlefair, S. P., Dhillon, V. S., Marsh, T. R., et al. 2008, MNRAS Lett., 391, L88
Lynch, C., Mutel, R. L., & Güdel, M. 2015, ApJ, 802, 106
Martín, E. L., Delfosse, X., Basri, G., et al. 1999, AJ, 118, 2466
Martín, E. L., Rebolo, R., & Magazzù, A. 1994, ApJ, 436, 262
McLean, M., Berger, E., Irwin, J., Forbrich, J., & Reiners, A. 2011, ApJ, 741, 27
McLean, M., Berger, E., & Reiners, A. 2012, ApJ, 746, 23
McMullin, J. P., Waters, B., Schiebel, D., Young, W., & Golap, K. 2007, in ASP Conf. Ser. 376, Astronomical Data Analysis Software and Systems XVI, ed. R. A. Shaw, F. Hill & D. J. Bell (San Francisco, CA: ASP), 127
Miles-Páez, P. A., Zapatero Osorio, M. R., & Pallé, E. 2015, A&A, in press (arxiv:1507.06902)
Mohanty, S., & Basri, G. 2003, ApJ, 583, 451
Mohanty, S., Basri, G., Shu, F., Allard, F., & Chabrier, G. 2002, ApJ, 571, 469
Morin, J., Donati, J. F., Petit, P., et al. 2010, MNRAS, 407, 2269
Nichols, J. D., Burleigh, M. R., Casewell, S. L., et al. 2012, ApJ, 760, 59
Offringa, A. R., de Bruyn, A. G., Biehl, M., et al. 2010, MNRAS, 405, 155
Offringa, A. R., van de Gronde, J. J., & Roerdink, J. B. T. M. 2012, A&A, 539, 95
Osten, R. A., Hawley, S. L., Bastian, T. S., & Reid, I. N. 2006, ApJ, 637, 518
Osten, R. A., Phan-Bao, N., Hawley, S. L., Reid, I. N., & Ojha, R. 2009, ApJ, 700, 1750
Pallavicini, R., & White, S. M. 1996, Proc. of the ESO-IRAM-NFRA-Onsala Workshop, Science with Large Millimetre Arrays, ed. P. A. Shaver (Berlin: Springer-Verlag), 268
Perley, R. A., & Butler, B. J. 2013, ApJS, 204, 19
Petrosian, V. 1985, ApJ, 299, 987
Ravi, V., Hallinan, G., Hobbs, G., & Champion, D. J. 2011, ApJL, 735, L2
Reid, I. N., Cruz, K. L., Kirkpatrick, J. D., et al. 2008, AJ, 136, 1290
Reid, I. N., Kirkpatrick, J. D., Liebert, J., et al. 2002, AJ, 124, 519
Reid, M. J., & Menten, K. M. 1997, ApJ, 476, 327
Reiners, A., & Basri, G. 2007, ApJ, 656, 1121
Reiners, A., & Basri, G. 2010, ApJ, 710, 924
Saar, S. H., & Brandenburg, A. 1999, ApJ, 524, 295
Salter, D. M., Hogerheijde, M. R., & Blake, G. A. 2008, A&A, 492, L21
Schmidt, S. J., Hawley, S. L., West, A. A., et al. 2015, AJ, 149, 158
Skrutskie, M. F., Cutri, R. M., Stiening, R., et al. 2006, AJ, 131, 1163
Stassun, K. G., Kratter, K. M., Scholz, A., & Dupuy, T. J. 2012, ApJ, 756, 47
Stelzer, B., Micela, G., Flaccomio, E., Neuhäuser, R., & Jayawardhana, R. 2006, A&A, 448, 293
Tinney, C. G. 1993, AJ, 105, 1169
Topka, K., & Marsh, K. A. 1982, ApJ, 254, 641
Treumann, R. 2006, A&ARv, 13, 229
West, A. A., Morgan, D. P., Bochanski, J. J., et al. 2011, AJ, 141, 97
Williams, J. P., & Cieza, L. A. 2011, ARA&A, 49, 67
Williams, P. K. G., & Berger, E. 2015, ApJ, 808, 189
Williams, P. K. G., Berger, E., & Zauderer, B. A. 2013, ApJL, 767, L30
Williams, P. K. G., Cook, B. A., & Berger, E. 2014, ApJ, 785, 9
Wolszczan, A., & Route, M. 2014, ApJ, 788, 23
Wu, C. S., & Lee, L. C. 1979, ApJ, 230, 621
Zarka, P. 1998, JGR, 103, 20159
Zhelezniakov, V. V. 1958, SvA, 2, 206